Plasmon-enhanced Kerr nonlinearity via subwavelength-confined anisotropic Purcell factors

2016 Nanotechnology 27 425205

(http://iopscience.iop.org/0957-4484/27/42/425205)

IOP Publishing Nanotechnology
Nanotechnology 27 (2016) 425205 (5pp) doi:10.1088/0957-4484/27/42/425205

Plasmon-enhanced Kerr nonlinearity via subwavelength-confined anisotropic Purcell factors

Juanjuan Ren[1], Hongyi Chen[1], Ying Gu[1,2], Dongxing Zhao[1], Haitao Zhou[2,3], Junxiang Zhang[2,3] and Qihuang Gong[1,2]

[1] State Key Laboratory for Mesoscopic Physics, Collaborative Innovation Center of Quantum Matter, Department of Physics, Peking University, Beijing 100871, People's Republic of China
[2] Collaborative Innovation Center of Extreme Optics, Shanxi University, Taiyuan, Shanxi 030006, People's Republic of China
[3] State Key Laboratory of Quantum Optics and Quantum Optics Devices, Institute of Opto-Electronics, Shanxi University, Taiyuan 030006, People's Republic of China

E-mail: ygu@pku.edu.cn

Received 17 July 2016, revised 18 August 2016
Accepted for publication 19 August 2016
Published 15 September 2016

Abstract

We theoretically investigate the enhancement of Kerr nonlinearity through anisotropic Purcell factors provided by plasmon nanostructures. In a three-level atomic system with crossing damping, larger anisotropism of Purcell factors leads to more enhanced Kerr nonlinearity in electromagnetically induced transparency windows. While for fixed anisotropic Purcell factors, Kerr nonlinearity with orthogonal dipole moments increases with the decrease of its crossing damping, and Kerr nonlinearity with nonorthogonal dipole moments is very sensitive to both the value of crossing damping and the orientation of the dipole moments. We design the non-resonant gold nanorods array, which only provides subwavelength-confined anisotropic Purcell factors, and demonstrate that the Kerr nonlinearity of cesium atoms close to the nanorods array can be modulated at the nanoscale. These findings should have potential application in ultracompact quantum logic devices.

Keywords: surface plasmon, Kerr nonlinearity, quantum coherence

(Some figures may appear in colour only in the online journal)

1. Introduction

Kerr nonlinearity, referring to the real part of the third-order susceptibility, has been studied widely for its potential application in quantum information [1–8]. It is desired to get large nonlinearity with small linear absorption under low light intensities [9, 10]. The enhanced Kerr nonlinearity can be obtained via such methods as electromagnetically induced transparency (EIT) [4], interaction of dark resonances [5], and spontaneously generated coherence (SGC) [6–8]. In addition, a strong localized field of metallic nanostructures can be used to enhance nonlinearity of metal itself or materials close to the metal, such as second-harmonic generation [11], third-harmonic generation [12, 13], optical frequency mixing [14] and high-harmonic generation [15]. Besides light confinement, large and anisotropic Purcell factors can be realized by carefully designing the metallic nanostructures, which have been studied in fluorescence enhancement [16, 17], quantum interference enhancement [18], the control of spontaneous emission spectra [19] and the control of double-trapping EIT spectra [20]. In previous work, the nonlinearity is greatly enhanced via SGC induced by anisotropic Purcell factors in four-level systems [7]. However, the effect of anisotropic Purcell factors themselves on the Kerr nonlinearity of three-level atoms in the vicinity of non-resonant plasmon nanostructures has not been explored yet.

In this paper, placing the three-level atoms with crossing damping close to a metallic nanostructure, we theoretically investigate the effects of anisotropic Purcell factors on the Kerr nonlinearity. The larger anisotropism of Purcell factors

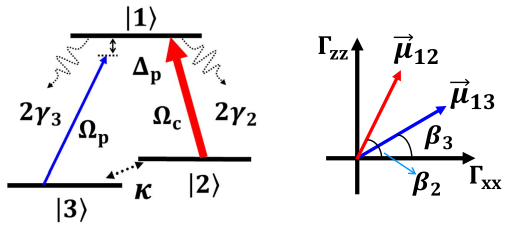

Figure 1. The schematic of a Λ-type three-level atomic system with the crossing damping κ between two near-degenerate lower levels $|2\rangle$ and $|3\rangle$. Γ_{xx} (Γ_{zz}) is the decay rate along the x (z) direction. β_2 (β_3) is the angle between the dipole moment $\vec{\mu}_{12}$ ($\vec{\mu}_{13}$) and the x axis.

leads to more enhanced Kerr nonlinearity. If the anisotropic Purcell factors are fixed, the Kerr nonlinearity with orthogonal dipole moments increases with the decrement of its crossing damping. While for nonorthogonal dipole moments, the Kerr nonlinearity is very sensitive to the orientation of dipole moment and the crossing damping. Note that here we focus on the impact of the anisotropic Purcell factors themselves on the Kerr nonlinearity. This is different from the previous studies in [7], where the key point is that the larger crossing damping induced by the anisotropic Purcell factors leads to larger Kerr nonlinearity. Available Λ-type systems can be found in the D1 line of cesium atoms. Using Green's tensor method [21, 22], we design the non-resonant gold nanorods array, which means what we utilize is only the anisotropic Purcell factors rather than its strong localized field. By changing the position of the cesium atoms relative to the gold nanorods array, the Kerr nonlinearity can be enhanced effectively at the nanoscale. These findings should have potential application in ultracompact quantum devices.

2. Method

The Λ-type three-level atomic system is shown in figure 1. A strong coupling field $\vec{E}_c$ with angular frequency of ω_c and a weak probe field $\vec{E}_p$ with ω_p couple the upper level $|1\rangle$ with two near-degenerate lower levels $|2\rangle$ and $|3\rangle$ respectively. The detunings $\Delta_c = \omega_{12} - \omega_c = 0$ and $\Delta_p = \omega_{13} - \omega_p$, where ω_{12} and ω_{13} are the frequencies of relevant atomic transitions. For simplicity, we assume the Rabi frequencies $\Omega_c = \vec{\mu}_{12} \cdot \vec{E}_c/2\hbar$ and $\Omega_p = \vec{\mu}_{13} \cdot \vec{E}_p/2\hbar$ are real, where the $\vec{\mu}_{1j} = \langle 1|-e\vec{r}|j\rangle$ $(j = 2, 3)$ is the matrix element of the electron-dipole moment between the levels $|1\rangle$ and $|j\rangle$. In anisotropic Purcell factors space, decay rates along the x (z) direction $\Gamma_{xx} = 3\gamma_0\lambda_{12}\,\mathrm{Im}\,G_{xx}$ ($\Gamma_{zz} = 3\gamma_0\lambda_{12}\,\mathrm{Im}\,G_{zz}$) are connected with imaginary parts of Green's tensor coefficients $G_{\beta\beta}$ with $\beta = x, y, z$, where $\gamma_0 = \mu^2\omega_{12}^3/(3\pi\epsilon_0\hbar c^3)$ is the decay rate in free vacuum [23, 24]. In particular, the condition that $\Gamma_{xx} = \Gamma_{zz} = \Gamma_0$ stands for the isotropic vacuum. β_2 (β_3) is the angle between the dipole moment $\vec{\mu}_{12}$ ($\vec{\mu}_{13}$) and the x axis. Thus the decay rate from level $|1\rangle$ to $|i\rangle$ is $2\gamma_i = \Gamma_{xx}cos^2\,\beta_i + \Gamma_{zz}\sin^2\beta_i$ $(i = 2, 3)$ and the crossing damping between two closely spaced levels $|2\rangle$ and $|3\rangle$ is $\kappa = \Gamma_{xx}\cos\beta_2\cos\beta_3 + \Gamma_{zz}\sin\beta_2\sin\beta_3$. The crossing damping originates from the interactions of two atomic transitions ($|1\rangle \leftrightarrow |2\rangle$ and $|1\rangle \leftrightarrow |3\rangle$) with the same electromagnetic vacuum, which has been studied in the spectral modification of spontaneous emission [19, 25–28]. Note that only the levels lie so closely that we need take the crossing damping into account.

Under the rotating-wave and dipole approximations, the density matrix in the interaction picture can be derived as follows:

$$\begin{aligned}
\dot{\rho}_{11} &= -2(\gamma_2+\gamma_3)\rho_{11} + i\Omega_p(\rho_{31}-\rho_{13}) + i\Omega_c(\rho_{21}-\rho_{12}),\\
\dot{\rho}_{33} &= 2\gamma_3\rho_{11} + i\Omega_p(\rho_{13}-\rho_{31}),\\
\dot{\rho}_{23} &= -i\Delta_p\rho_{23} + \kappa\rho_{11} + i\Omega_c\rho_{13} - i\Omega_p\rho_{21},\\
\dot{\rho}_{13} &= -(\gamma_2+\gamma_3+i\Delta_p)\rho_{13} - i\Omega_p(\rho_{11}-\rho_{33}) + i\Omega_c\rho_{23},\\
\dot{\rho}_{12} &= -(\gamma_2+\gamma_3)\rho_{12} + i\Omega_p\rho_{32} - i\Omega_c(\rho_{11}-\rho_{22}),
\end{aligned} \tag{1}$$

which satisfies $\rho_{11} + \rho_{22} + \rho_{33} = 1$ and $\rho_{ij}^* = \rho_{ji}$. Relations between the susceptibilities and density matrix elements can be obtained by combining the two expressions of polarization intensity. The first is $P = \varepsilon_0(E_p\chi + E_p^*\chi^*)/2$, where χ is the susceptibility of the atomic medium. The second is the quantum average of N atoms' dipole moments $P = N(\mu_{31}\rho_{13} + \mu_{13}\rho_{31})$. Furthermore, to derive the linear and nonlinear susceptibilities, steady-state solution is given, where the iterative method is utilized and the density matrix elements can be written as $\rho_{mn} = \rho_{mn}^{(0)} + \rho_{mn}^{(1)} + \rho_{mn}^{(2)} + \rho_{mn}^{(3)} + \cdots$. The probe field is much weaker than the coupling field, so the zeroth order solution is $\rho_{33}^{(0)} = 1$, and other elements are equal to zero. Deducing the matrix elements up to the third order, the first-order susceptibility $\chi^{(1)}$ and third-order susceptibility $\chi^{(3)}$ can be attained as the following:

$$\chi^{(1)} = \frac{2N|\vec{\mu}_{13}|^2}{\varepsilon_0\hbar\Omega_p}\rho_{13}^{(1)},\ \chi^{(3)} = \frac{2N\,|\vec{\mu}_{13}|^4}{3\varepsilon_0\hbar^3\Omega_p^3}\rho_{13}^{(3)}, \tag{2}$$

and the total susceptibility χ is

$$\chi = \chi^{(1)} + 3|E_p|^2\chi^{(3)}. \tag{3}$$

3. Results and discussion

First, we will focus on the influence of the anisotropic Purcell factors on the Kerr nonlinearity. The first-order and third-order susceptibilities against the detuning Δ_p with various Purcell factors are shown in figure 2. Here, the crossing damping κ is zero through keeping $\vec{\mu}_{13}$ parallel to the x-axis and $\vec{\mu}_{12}$ parallel to the z-axis. The Rabi frequency is fixed at $\Omega_c = 2.0\gamma_0$ in the following. Three cases are explored: $\Gamma_{xx} = \Gamma_{zz} = \gamma_0$ (black curves), $\Gamma_{xx} = 0.5\gamma_0$, $\Gamma_{zz} = 1.5\gamma_0$ (red curves) and $\Gamma_{xx} = 0.25\gamma_0$, $\Gamma_{zz} = 1.75\gamma_0$ (blue curves). The first-order susceptibilities are completely the same (figures 2(a) and (b)) because they are inversely proportional to the sum of two transitions' decay rates and the value is $2\gamma_2 + 2\gamma_3 = 2.0\gamma_0$ in three cases. Close to the EIT window, the Kerr nonlinearity with anisotropic Purcell factors can be up to four times larger than that in isotropic vacuum

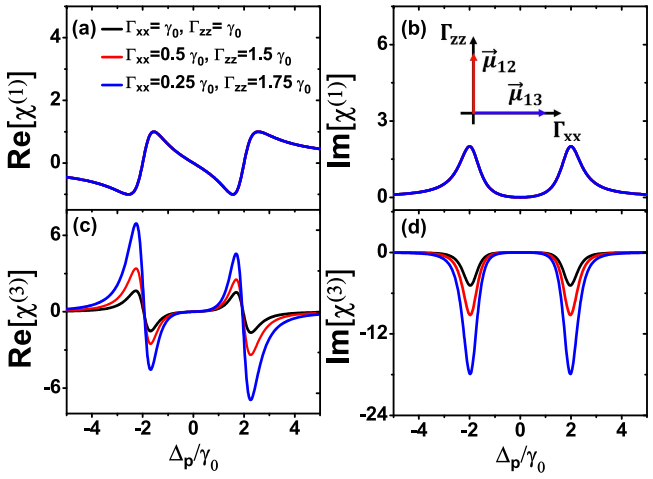

Figure 2. Enhanced Kerr nonlinearity via anisotropic Purcell factors under perpendicular dipole moments. (a, b) Linear and (c, d) nonlinear susceptibilities of probe field against the probe detuning. The inset in (b) shows the orientation of transition dipole moments. One can see that Kerr nonlinearity increases with an increment of Purcell factors anisotropism though the linear dispersion and absorption curves are the same.

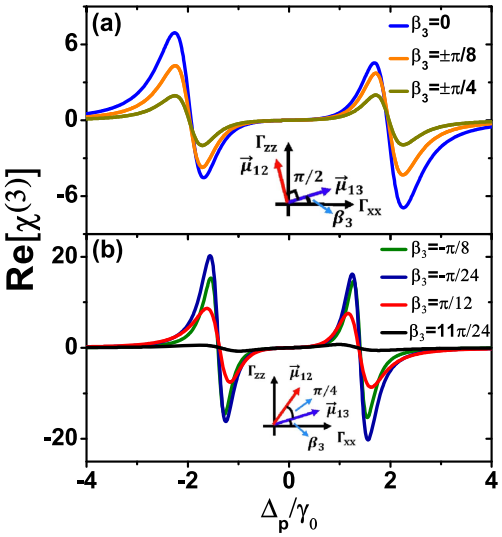

Figure 3. Enhanced Kerr nonlinearity with different orientations of dipole moments and the fixed anisotropic Purcell factors $\Gamma_{xx} = 0.25\gamma_0, \Gamma_{zz} = 1.75\gamma_0$. The angles between two dipole moments are fixed at $\frac{\pi}{2}$ (a) and $\frac{\pi}{4}$ (b). With perpendicular dipole moments, when $\beta_3 = 0$, $\beta_2 = \frac{\pi}{2}$, the Kerr nonlinearity reaches the maximum. While with nonorthogonal dipole moments in (b), the Kerr nonlinearity is the maximum when $\beta_3 = -\frac{\pi}{24}$, $\beta_2 = \frac{5\pi}{24}$.

(figure 2(c)). Meanwhile, there are nonlinear gains because the imaginary parts of the third-order susceptibilities are negative (figure 2(d)). Note that the results in isotropic vacuum are in agreement with that of [6]. Further calculations indicate that the Kerr nonlinearities for nonorthogonal dipole moments also increase with the increment of the anisotropism of Purcell factors although the crossing damping is non-zero. In brief, larger anisotropism of Purcell factors leads to larger Kerr nonlinearity.

Then we fix the Purcell factors as $\Gamma_{xx} = 0.25\gamma_0$, $\Gamma_{zz} = 1.75\gamma_0$ to investigate the effect of crossing damping on the Kerr nonlinearity. The Kerr nonlinearity with orthogonal and nonorthogonal dipole moments are shown in figures 3(a) and (b). When $\beta_2 - \beta_3 = \frac{\pi}{2}$, we discuss five cases with various relative orientation of dipole moments: $\beta_3 = 0$ (blue curve), $\beta_3 = \pm\frac{\pi}{8}$ (orange curves), $\beta_3 = \pm\frac{\pi}{4}$ (dark yellow curves) with crossing dampings' absolute values of 0, 0.53 and 0.75. The Kerr nonlinearity reaches the maximum when $\beta_3 = 0$, which indicates that the smaller crossing damping leads to the larger Kerr nonlinearity. Note that in isotropic vacuum, the larger crossing damping generally leads to larger Kerr nonlinearity because of the same decay rates from the excited level $|1\rangle$ to both ground levels $|2\rangle$ and $|3\rangle$ [6]. In addition, the crossing damping induced by anisotropic Purcell factors in the four-level system greatly enhanced the nonlinearity [7]. However, here in the three-level system with anisotropic Purcell factors, the crossing damping suppresses the enhancement of Kerr nonlinearity.

While for $\beta_2 - \beta_3 = \frac{\pi}{4}$, we consider four cases: $\beta_3 = -\frac{\pi}{8}$ (olive green curve), $\beta_3 = -\frac{\pi}{24}$ (black curve), $\beta_3 = \frac{\pi}{12}$ (red curve), $\beta_3 = \frac{11\pi}{24}$ (royal blue curve) with crossing dampings' absolute values of 0.043, 0.057, 0.51 and 1.35. When $\beta_3 = -\frac{\pi}{24}$ ($\beta_3 = \frac{11\pi}{24}$), the Kerr nonlinearity is the maximum (minimum). Different from the case with perpendicular dipole moments, the smaller crossing damping does not necessarily lead to larger Kerr nonlinearity due to the combined effect of the crossing damping and the orientation of dipole moment. In addition, comparing the figures 3(a) and (b), the smaller angle between dipole moments leads to larger Kerr nonlinearity, which is in agreement with that of the isotropic situation. In brief, the Kerr nonlinearity can be effectively enhanced via changing anisotropic Purcell factors and the orientation of dipole moments.

Finally, in order to obtain the enhanced Kerr nonlinearity with anisotropic Purcell factors at the subwavelength scale, we apply the above mechanisms to cesium atoms in the vicinity of surface plasmon structures. Available Λ-type system can be found in $D1$ line of cesium atoms, whose resonant wavelength is 895 nm. Two neighboring Zeeman sublevels of $6^2S_{1/2}$, $F = 4$ are set as level $|2\rangle$ and $|3\rangle$, and one Zeeman sublevel of $6^2P_{1/2}$, $F' = 3$ is set as level $|1\rangle$. The custom-designed plasmon nanostructurs is a gold nanorods array with size of $100 \times 50 \times 50$ nm^3 and gap of 25 nm (figure 4(a)), whose resonant wavelength is 730 nm, far from that of the cesium atom's $D1$ line. Different from a previous study [7], we only utilize the anisotropic Purcell factors provided by the nanostructures rather than its localized field. The Purcell factors at $\lambda = 895$ nm are numerically calculated from $z = -200$ nm to $z = 150$ nm using Green's tensor method with the mesh of 25 nm. Specifically, the Purcell factors' distributions at $z = 50$ nm are shown in figures 4(b) and (c). Increasing the distance from the nanostructures to infinite, Purcell factors approach isotropic vacuum value $1.0\gamma_0$.

Taking advantage of the anisotropic Purcell factors of the gold nanorods array, we investigate the Kerr nonlinearity of

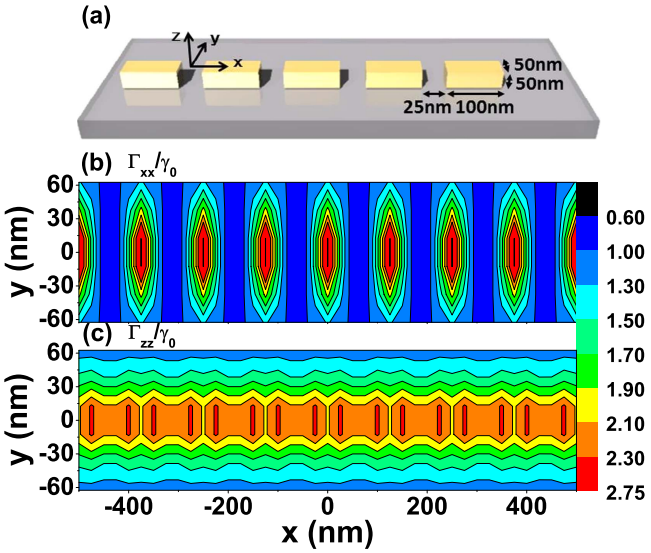

Figure 4. (a) The plasmon nanostructure consisting of nanorods array with size of $100 \times 50 \times 50$ nm^3 and gap of 25 nm. (b) and (c) Distribution of Purcell factors Γ_{xx}/γ_0 and Γ_{zz}/γ_0 at $z = 50$ nm. Anisotropic Purcell factors are obtained, which can be used to enhance the Kerr nonlinearity.

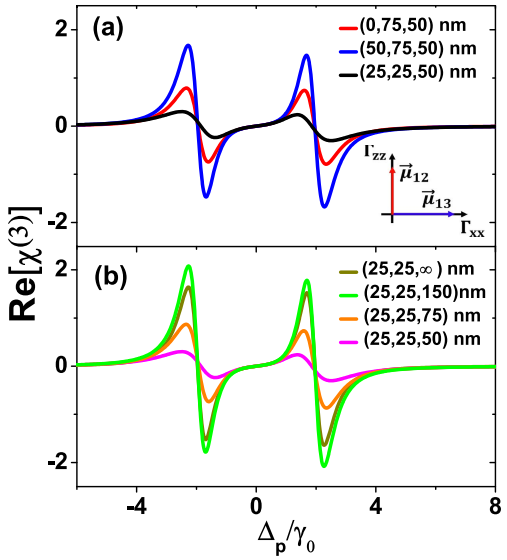

Figure 5. Kerr nonlinearity of cesium atoms with anisotropic Purcell factors provided by the designed gold nanorods array for three positions at $z = 50$ nm (a), and for $z = 50$, 75, 150, ∞ nm, $x = y = 25$ nm (b). The case (25, 25, ∞) nm represents the homogeneous vacuum. The Kerr nonlinearity can be modulated by changing the position of the atoms relative to the plasmon nanostructures.

cesium atoms nearby. In the xy-plane of $z = 50$ nm, the Kerr nonlinearities with perpendicular dipole moments at points (0, 75, 50) nm (red curve), (50, 75, 50) nm (blue curve), (25, 25, 50) nm (black curve) are shown in figure 5(a). The Kerr nonlinearities at the positions with $z = 50$, 75, 150, ∞ nm are illustrated in figure 5(b). One can find that it is convenient to modulate the Kerr nonlinearity by changing the atoms' position relative to the plasmon nanostructures. In brief, anisotropic Purcell factors provided by custom-designed plasmon nanostructures can enhance the Kerr nonlinearity of the atoms at the nanoscale, and the mechanism of enhanced Kerr nonlinearity can be used in other custom-designed quantum systems close to plasmon nanostructures.

Experimentally fabricating the designed periodic plasmon nanostructures is promising with current techniques. Except for the Zeeman sublevels of the cesium, the three-level atomic system can be found in the quantum dot and nitrogen-vacancy center [29]. Accurately controlling the atoms' position relative to structures is challenging, but taking advantage of the plasmonic nanostructures to trap the atoms has been studied both theoretically and experimentally [30–32]. So, experimental realization of our protocol is promising in the near future.

4. Conclusion

We have theoretically analyzed the plasmon-enhanced Kerr nonlinearity of a three-level system via subwavelength-confined anisotropic Purcell factors. The Kerr nonlinearities increase with the increment of the anisotropism of Purcell factors. If the anisotropic Purcell factors are fixed, small crossing damping leads to large Kerr nonlinearity for orthogonal dipole moments. While for nonorthogonal dipole moments, both the crossing damping and the orientation of dipole moment influence the Kerr nonlinearity. Furthermore, we have investigated the Kerr nonlinearity of cesium atoms with the custom-designed gold nanorods array. The nonlinearity can be effectively enhanced by changing the atoms' relative position to the nanostructures. Besides plasmon structures, the mechanism of the enhanced Kerr nonlinearity with anisotropic Purcell factors can be extended to other nanostructures such as metasurface, which can also provide anisotropic Purcell factors [33]. The enhanced nonlinearity at the nanoscale in hybrid quantum emitter-plasmonic nanostructure systems provides a new platform for nonlinear optics, which has potential applications in ultra-compact quantum logic devices, all-optical switches and nonlinear devices.

Acknowledgments

This work was supported by the National Key Basic Research Program under Grant No. 2013CB328700, and by the National Natural Science Foundation of China under Grant Nos. 11525414, 11374025, and 91221304.

References

[1] Wang H, Goorskey D and Xiao M 2001 Enhanced Kerr nonlinearity via atomic coherence in a three-level atomic system *Phys. Rev. Lett.* **69** 073601

[2] Han Y, Xiao J, Liu Y, Zhang C, Wang H, Xiao M and Peng K 2008 Interacting dark states with enhanced nonlinearity in an ideal four-level tripod atomic system *Phys. Rev.* A **77** 023824

[3] Sheng J, Yang X, Wu H and Xiao M 2011 Modified self-Kerr-nonlinearity in a four-level N-type atomic system *Phys. Rev.* A **84** 053820

[4] Schmidt H and Imamoğlu A 1996 Giant Kerr nonlinearities obtained by electromagnetically induced transparency *Opt. Lett.* **21** 1936–8

[5] Niu Y, Gong S, Li R, Xu Z and Liang X 2005 Giant Kerr nonlinearity induced by interacting dark resonances *Opt. Lett.* **30** 3371–3

[6] Niu Y and Gong S 2006 Enhancing Kerr nonlinearity via spontaneously generated coherence *Phys. Rev.* A **73** 053811

[7] Chen H, Ren J, Gu Y, Zhao D, Zhang J and Gong Q 2015 Nanoscale Kerr nonlinearity enhancement using spontaneously generated coherence in plasmonic nanocavity *Sci. Rep.* **5** 18315

[8] Evangelou S, Yannopapas V and Paspalakis E 2014 Modification of Kerr nonlinearity in a four-level quantum system near a plasmonic nanostructure *J. Mod. Opt.* **61** 1458–64

[9] Hemmer P R, Katz D P, Donoghue J, Cronin-Golombet M, Shahriar M S and Kumar P 1995 Efficient low-intensity optical phase conjugation based on coherent population trapping in sodium *Opt. Lett.* **20** 982–4

[10] Harris S E and Hau L V 1999 Nonlinear optics at low light levels *Phys. Rev. Lett.* **82** 4611

[11] Bouhelier A, Beversluis M, Hartschuh A and Novotny L 2003 Near-field second-harmonic generation induced by local field enhancement *Phys. Rev. Lett.* **90** 013903

[12] Lippitz M, van Dijk M A and Orrit M 2005 Third-harmonic generation from single gold nanoparticles *Nano Lett.* **5** 799–802

[13] Aouani H, Rahmani M, Navarro-Cía M and Maier S A 2014 Third-harmonic-upconversion enhancement from a single semiconductor nanoparticle coupled to a plasmonic antenna *Nat. Nanotechnol* **9** 290–4

[14] Renger J, Quidant R, van Hulst N and Novotny L 2010 Surface-enhanced nonlinear four-wave mixing *Phys. Rev. Lett.* **104** 046803

[15] Kim S, Jin J, Kim Y-J, Park I-Y, Kim Y and Kim S-W 2008 High-harmonic generation by resonant plasmon field enhancement *Nature* **453** 757–60

[16] Kühn S, Håkanson U, Rogobete L and Sandoghdar V 2006 Enhancement of single-molecule fluorescence using a gold nanoparticle as an optical nanoantenna *Phys. Rev. Lett.* **97** 017402

[17] Tam F, Goodrich G P, Johnson B R and Halas N J 2007 Plasmonic enhancement of molecular fluorescence *Nano Lett.* **7** 496–501

[18] Yannopapas V, Paspalakis E and Vitanov N V 2009 Plasmon-induced enhancement of quantum interference near metallic nanostructures *Phys. Rev. Lett.* **103** 063602

[19] Gu Y, Wang L, Ren P, Zhang J, Zhang T, Martin O J F and Gong Q 2012 Surface-plasmon-induced modification on the spontaneous emission spectrum via subwavelength-confined anisotropic Purcell factor *Nano Lett.* **12** 2488–93

[20] Wang L, Gu Y, Chen H, Zhang J-Y, Cui Y, Gerardot B D and Gong Q 2013 Polarized linewidth-controllable double-trapping electromagnetically induced transparency spectra in a resonant plasmon nanocavity *Sci. Rep.* **3** 02879

[21] Gu Y, Chen L, Zhang H and Gong Q 2008 Resonance capacity of surface plasmon on subwavelength metallic structures *Europhys. Lett.* **83** 27004

[22] Martin O J F, Girard C and Dereux A 1995 Generalized field propagator for electromagnetic scattering and light confinement *Phys. Rev. Lett.* **74** 526

[23] Barnett S M, Huttner B, Loudon R and Matloob R 1996 Decay of excited atoms in absorbing dielectrics *J. Phys. B: At. Mol. Opt. Phys.* **29** 3763–80

[24] Gu Y, Huang L, Martin O J F and Gong Q 2010 Resonance fluorescence of single molecules assisted by a plasmonic structure *Phys. Rev.* B **81** 193103

[25] Zhu S-Y and Scully M O 1996 Spectral line elimination and spontaneous emission cancellation via quantum interference *Phys. Rev. Lett.* **76** 388

[26] Lee H, Polynkin P, Scully M O and Zhu S-Y 1997 Quenching of spontaneous emission via quantum interference *Phys. Rev.* A **55** 4454

[27] Zhou P and Swain S 1996 Ultranarrow spectral lines via quantum interference *Phys. Rev. Lett.* **77** 3995

[28] Paspalakis E and Knight P L 1998 Phase control of spontaneous emission *Phys. Rev. Lett.* **81** 293

[29] Santori C *et al* 2006 Coherent population trapping in diamond N-V centers at zero magnetic field *Opt. Express* **14** 7986

[30] Chang D E, Thompson J D, Park H, Vuletic V, Zibrov A S, Zoller P and Lukin M D 2009 Trapping and manipulation of isolated atoms using nanoscale plasmonic structures *Phys. Rev. Lett.* **103** 123004

[31] Stehle C, Bender H, Zimmermann C, Kern D, Fleischer M and Sebastian S 2011 Plasmonically tailored micropotentials for ultracold atoms *Nat. Photon.* **5** 494

[32] Stehle C, Zimmermann C and Sebastian S 2014 Cooperative coupling of ultracold atoms and surface plasmons *Nat. Phys.* **10** 937

[33] Jha P K, Ni X, Wu C, Wang Y and Zhang X 2015 Metasurface-enabled remote quantum interference *Phys. Rev. Lett.* **115** 025501